A Constant Voltage MPPT Method for a Solar Powered Boost Converter with DC Motor Load

Aleck W. Leedy
Dept. of Engineering & Physics
Murray State University
Murray, KY 42071-3346, USA
e-mail: aleedy@murraystate.edu

Liping Guo
Dept. of Technology
Northern Illinois University
DeKalb, IL 60115-2854, USA
e-mail: lguo@niu.edu

Kennedy A. Aganah
Dept. of ECE
Tennessee Tech University
Cookeville, TN 38505, USA
e-mail: adinbo@gmail.com

***Abstract*— A constant voltage maximum power point (MPP) algorithm that automatically adjusts the reference voltage to account for varying environmental conditions is presented. A simple (and inexpensive) analog feedforward PWM controller is developed to continuously track the MPP of a solar cell array as the weather conditions vary. The solar array source is configured such that its open-circuit voltage is sampled without breaking the entire source from the load as is the case with other constant voltage MPP algorithms. MATLAB/Simulink simulations are presented to demonstrate the performance of the proposed MPP algorithm. Simulation results collaborated with experimental results using a DC motor load.**

***Keywords*-Maximum power point (MPP); boost converter; solar cell array; and pulsewidth modulation (PWM).**

I. INTRODUCTION

Sustainable energy sources like solar, wind, and fuel cells are becoming increasingly important as environmentally friendly alternatives to the traditional energy sources such as fossil fuels. However, these environmentally friendly sources are difficult to tap, store, and use. Successful application of these sustainable sources depends on being able to maximize efficiency in both conversion and energy storage. Maximum power point (MPP) tracking techniques are employed in solar array powered systems to optimize the power from the array output that depends on solar insolation, cell temperature, and load levels. Many different techniques have been proposed and implemented to various degrees of success. Trishan and Chapman [1] suggest that there are at least nineteen distinct methods with many variations and implementations of each method. However, in practice, the most commonly implemented methods include power matching, perturb-and-observe (P&O), incremental conductance (IncCond), ripple correlation control (RCC), constant voltage, and constant current methods.

The power matching approach [2,3] pre-selects solar panels with specific power characteristics or configurations that can be matched well with specific loads. The load is normally direct-coupled to the solar panel, avoiding any complex control circuitry. However, the approach only approximates the MPP, and the true MPP is never achieved. It is also too specific since, for each load requirement, the solar module must be extensively characterized.

The P&O [4, 5] is the most widely used method. The technique uses an iterative process that perturbs the operating point of the solar power system in order to find the direction of change maximizing power. Periodically, the operating voltage of the solar module is changed to move it towards the maximum power point using power feedback and/or feedforward control. The method has been shown to work well when insolation does not vary quickly with time. Under rapidly changing conditions, the P&O method quickly fails due to a divergence from the MPP. Improvements have been made to this method.

The shortcomings of the P&O method can be improved by using the incremental conductance method. The incremental conductance algorithm [6] makes use of the fact that the slope of the solar module P-V curve is zero at the MPP, positive on the left of the MPP, and negative on the right of the MPP. The IncCond method has the advantage over the P&O of not oscillating around the MPP under rapidly changing environmental conditions, but has a more complex circuitry. The accuracy of the method depends on the iteration size, which is usually fixed for the conventional IncCond method. There are many improvements to the conventional IncCond [7]. Liu et al. [8] employ a variable step size to increase the accuracy and a faster convergence to the MPP.

The ripple correlation control method [9,10] makes use of the current or voltage ripples inherent in power converters, as these ripples provide some information about the system operating point. RCC has the advantage of not introducing any external disturbance into the system, but makes use of the current or voltage ripple already present in the system. The method converges asymptotically at maximum speed to the MPP without the benefit of any module parameters or measurement.

The simplest and fastest methods to achieve MPP are the constant voltage [11,12] and constant current [12] methods. Both techniques assume a linear dependence between the module current (or voltage) corresponding to maximum power and the module's short-circuit current (or open-circuit voltage). The short fall of both methods is that constant environmental conditions are assumed, and the true MPP is not always achieved. Improved versions [12,13] use online tracking algorithms to detect short-circuit currents and open-circuit voltages.

978-1-4673-1375-9/12/$31.00 ©2012 IEEE

The purpose of this paper is to design an analog maximum power point (MPP) tracker for the system shown in Fig. 1. The system in Fig. 1 is comprised of a solar cell array, a DC-DC boost converter, a pulse width modulated controller, and a load. Specifically, a four solar panel array configuration is employed to power the load. The norm nowadays is towards microprocessor-based MPP trackers that are often relatively expensive. In this paper, a simple (and inexpensive) analog feedforward PWM controller is developed to continuously track the MPP of the solar cell array in Fig. 1 as the weather conditions vary. The solar array source is configured such that its open-circuit voltage is sampled without breaking the entire source from the load as is the case with other constant voltage MPP algorithms. MATLAB/Simulink simulations and experimental analyses are presented to demonstrate the performance of the system in Fig. 1.

II. SYSTEM ANALYSIS

The solar cell array – converter connection for the proposed system to be studied with a DC motor load attached is shown in Fig. 2. The boost converter in Fig. 2 was operated in the continuous conduction mode for all analysis presented in this paper. Switch S3 switches at a low frequency with the assumption that the environmental changes take a few seconds. The circuit must have an extra driver dedicated to switch S3 so that it can open up to measure the open circuit voltage. Two modes of operation result depending on the position of the switches and the conduction of the diode. The equations for Mode I (S1=S3=1, and S2=0) can be written as follows:

$$\dot{i}_{in} = -\frac{(r_L + r_{ds1})}{L} i_{in} + \frac{v_i}{L} \tag{1}$$

$$\dot{v}_C = \frac{-i_a}{C} \tag{2}$$

$$\dot{i}_a = -\frac{(R_m + r_C)}{L_m} i_a - \frac{K_m}{L_m}\omega + \frac{1}{L_m} v_C \tag{3}$$

and

$$\dot{\omega} = \frac{K_m}{J} i_a - \frac{B}{J}\omega - \frac{T_L}{J} \tag{4}$$

where v_i is the boost converter input voltage, i_{in} is the input current of the boost converter, v_C is the capacitor voltage, L is the inductance of the inductor, r_L is the inductor resistance, C is the capacitance of the capacitor, r_C is the capacitor equivalent series resistance (ESR), $r_{DS,1}$ is the switch ON resistance, R_m is the total armature circuit resistance, L_m is the total armature circuit inductance, ω is the motor angular frequency, i_a is the armature current, B is the viscous friction constant, T_L is the load torque, J is the moment of inertia, and K_m is the back emf constant.

The equations for Mode II (S1=0, and S2=S3=1) can be written as follows:

$$\dot{i}_{in} = -\frac{(r_L + r_C)}{L} i_{in} + \frac{r_C}{L} i_a - \frac{1}{L} v_C + \frac{v_i}{L} \tag{5}$$

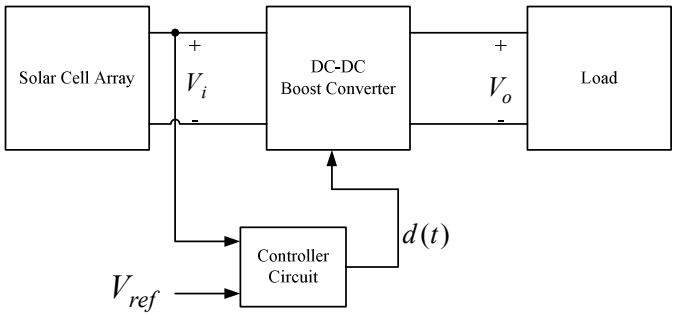

Figure 1. Solar Powered System Model.

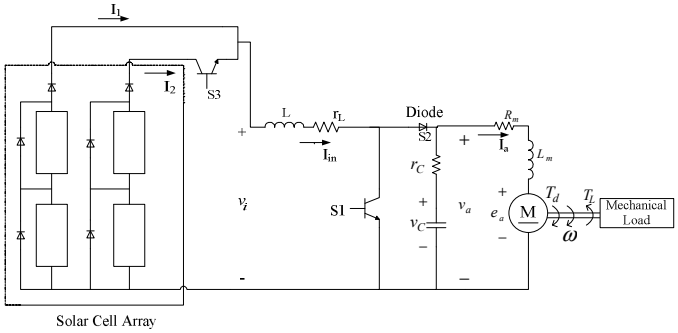

Figure 2. Solar cell array – converter connection.

$$\dot{v}_C = \frac{1}{C} i_{in} - \frac{1}{C} i_a \tag{6}$$

$$\dot{i}_a = -\frac{(R_m + r_C)}{L_m} i_a + \frac{r_C}{L_m} i_{in} - \frac{K_m}{L_m}\omega + \frac{1}{L_m} v_C \tag{7}$$

and

$$\dot{\omega} = \frac{K_m}{J} i_a - \frac{B}{J}\omega - \frac{T_L}{J} . \tag{8}$$

The state space averaging method can be used to combine (1-8) into one set of equations that will represent the dynamics of the system shown in Fig. 2. The four equations that result can be written as:

$$\dot{i}_{in} = -\frac{(r_L + dr_{DS,1} + (1-d)r_C)}{L} i_{in} + \frac{r_C}{L}(1-d) i_a - \frac{1}{L}(1-d) v_C + \frac{v_i}{L} \tag{9}$$

$$\dot{v}_C = -\frac{1}{C} i_a + \frac{1}{C}(1-d) i_{in} \tag{10}$$

$$\dot{i}_a = -\frac{(R_m + r_C)}{L_m} i_a + \frac{r_C}{L_m}(1-d) i_{in} - \frac{K_m}{L_m}\omega + \frac{1}{L_m} v_C \tag{11}$$

and

$$\dot{\omega} = \frac{K_m}{J} i_a - \frac{B}{J}\omega - \frac{T_L}{J} . \tag{12}$$

where d represents the duty cycle of switch S1.

III. PWM FEEDFORWARD CONTROLLER

Fig. 3 shows the small-signal model of the feedforward controller loop. The controller loop comprises the error

amplifier, the PWM modulator, and the boost converter power stage. The instantaneous input and open-circuit voltages are sensed and scaled down to appropriate levels. The difference between them is then fed to the error amplifier and amplified. The amplified error or control signal is what the PMW modulator uses to generate the PWM signal.

The control voltage $v_e(t)$ can be modeled by a DC component and a small signal component as [17]:

$$v_e(t) = V_e + \tilde{v}_e(t) \tag{13}$$

where $v_e(t)$ is in the range between zero and $\hat{V}_r$, as shown in Fig. 4. In this representation of the control signal, $\tilde{v}_e(t)$ is a sinusoidal ac perturbation component in the control voltage at a frequency f, where f is much smaller than the switching frequency (f_s). The ac perturbation in the control voltage can be expressed as:

$$\tilde{v}_e = a\sin(\omega t - \phi) \tag{14}$$

where a and ϕ are the amplitude and phase angle respectively.

In Fig. 4, the instantaneous switch duty cycle can be expressed as follows:

$$d(t) = \begin{cases} 1.0 & if\ v_e(t) \geq v_r(t) \\ 0 & if\ v_e(t) < v_r(t) \end{cases} . \tag{15}$$

The instantaneous switch duty cycle as derived in [17] can be written as:

$$d(t) = d_0 + \Delta d \tag{16}$$

where d_0 is the average duty cycle.

Small-signal analysis of the system in Fig. 2 produces the following equations:

$$\begin{bmatrix} \Delta i_{in} \\ \Delta v_c \\ \Delta i_a \\ \Delta \omega \end{bmatrix} = (sI - A)^{-1} B\Delta d + (sI - A)^{-1} U\Delta v_i \tag{17}$$

where

$$A = \begin{bmatrix} -\frac{(r_L + d_o r_{DS1} + (1-d_o)r_C)}{L} & -\frac{1-d_o}{L} & \frac{r_C(1-d_o)}{L} & 0 \\ \frac{1-d_o}{C} & 0 & -\frac{1}{C} & 0 \\ \frac{r_C(1-d_o)}{L_m} & \frac{1}{L_m} & -\frac{(R_m + r_C)}{L_m} & -\frac{K_m}{L_m} \\ 0 & 0 & \frac{K_m}{J} & -\frac{B}{J} \end{bmatrix},$$

$$B = \begin{bmatrix} -\frac{I_{in}(r_{DS1} - r_C) - I_a r_C + V_C}{L} \\ -\frac{I_{in}}{C} \\ -\frac{r_C I_{in}}{L_m} \\ 0 \end{bmatrix},$$

and

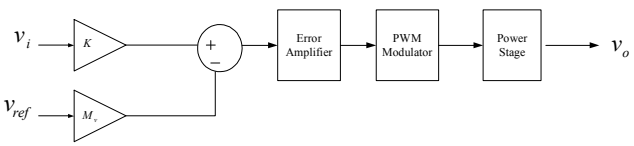

Figure 3. Block diagram of the feedforward controller.

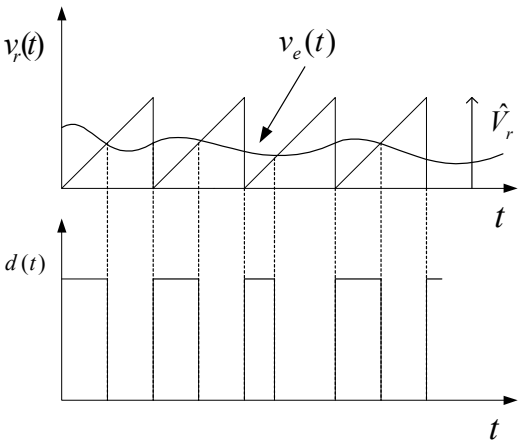

Figure 4. Comparator signals.

$$U = \begin{bmatrix} \frac{1}{L} \\ 0 \\ 0 \\ 0 \end{bmatrix}.$$

The following state equations result:

$$\begin{bmatrix} \Delta \dot{i}_{in} \\ \Delta \dot{v}_c \\ \Delta \dot{i}_a \\ \Delta \dot{\omega} \end{bmatrix} = A \begin{bmatrix} \Delta i_{in} \\ \Delta v_C \\ \Delta i_a \\ \Delta \omega \end{bmatrix} + B\Delta d + U\Delta v_i . \tag{18}$$

The proposed control method requires detecting the solar array output voltage variation with respect to its open-circuit voltage and adjusting the duty cycle to shift the system operating point towards the MPP. The small-signal input-to-output transfer function of the system, $T_{ff}(s)$, is found as follows:

$$G_{v_c v_i}(s) = \left.\frac{\Delta v_c(s)}{\Delta v_i(s)}\right|_{\Delta d = 0} = [0\ 1\ 0\ 0]\ [sI - A]^{-1} U \tag{19}$$

$$G_{v_c d}(s) = \left.\frac{\Delta v_c(s)}{\Delta d(s)}\right|_{\Delta v_i = 0} = [0\ 1\ 0\ 0][sI - A]^{-1} B \tag{20}$$

$$T_{ff}(s) = G_{v_c v_i}(s) + T_m G_{v_i d}(s) \tag{21}$$

where

$$T_m = -\frac{1}{\hat{V}_r}.$$

IV. MAXIMUM POWER POINT TRACKING

In Fig. 5, the solar powered system of Fig. 1 is modeled by a Thévenin equivalent network [10, 16] that comprises a voltage source (v_{pv}), in series with a resistance (r_{pv}) that represents the solar array. The input voltage and the equivalent input resistance of the power stage are modeled by v_i and r_i respectively. Assuming a lossless power stage, the input power will equal the output power as follows:

$$P_i = P_o = \frac{v_i^2}{r_i}. \tag{22}$$

The maximum power transfer condition dictates that at the MPP, there should be input-to-output impedance matching as follows:

$$r_{pv} = r_i = \frac{v_{pv}}{i_{pv}} = \frac{v_i}{i_i}. \tag{23}$$

If the input-output balance conditions are considered, r_i is dependent on the load resistance R and the voltage conversion ratio $M = \frac{v_o}{v_i}$. It follows from (22) that

$$r_i = \frac{R}{M^2} = R(1-d)^2. \tag{24}$$

It also follows from (23) and (24) that

$$v_i = i_i R(1-d)^2. \tag{25}$$

For a boost converter operating in CCM,

$$i_i = \frac{i_o}{1-d}, \tag{26}$$

and

$$v_i = i_o R(1-d) = v_o(1-d). \tag{27}$$

Equation (27) satisfies the condition for MPP and will be the basis for the design of the MPP tracking system.

In this paper, the small pilot panel used in Tarig and Asghar [13] will be replaced with a panel of equivalent characteristics as the main solar arrays (but this time connected in parallel with the main supply). A switch is connected in series with the new pilot array so that periodically, the switch opens and the open-circuit voltage is measured. The value of the open-circuit voltage is the reference voltage for the PWM modulator. The reference voltage in this scheme is dynamically tracked online, avoiding the need to break the main circuit as done in the conventional constant voltage algorithms.

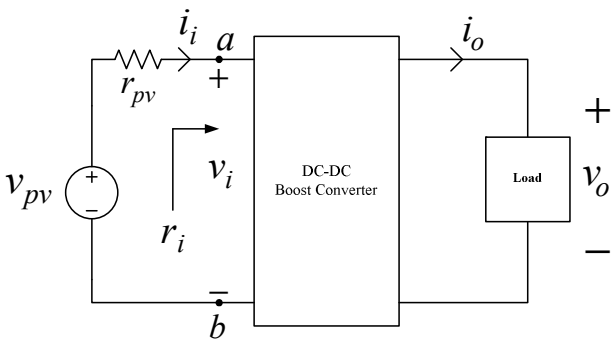

Figure 5. Equivalent circuit of a solar powered load.

V. MATLAB/SIMULINK SYSTEM MODEL

The state-space parameters A, B, and C can be found using (17). For the simulations presented in this section, the system in Fig. 2 had the following parameters: L=1.5 mH, r_L= 500 $m\Omega$, C=33 μF, r_C= 1$m\Omega$, $r_{DS,I}$= 200 $m\Omega$, R_m=8Ω, L_m=33mH, J=0.003835 kg m^2, B=0.001 N-ms/rad, K_m=0.67V/rad/s, and ω=1800 RPM. This enables the steady-state transfer functions to be determined by solving the state space equations. Fig. 6-8 illustrate the simulations of the solar cell powered system characteristics using Simulink. Fig. 6 shows the small signal transient output voltage as a response to a step change in the input voltage (0-1V) for the boost converter with feedforward control. It can be seen in Fig. 6 that the controller has a good capability to keep the output voltage stable. Fig. 7 - Fig. 9 depict the system behavior as a response to a 77-volt step input.

VI. EXPERIMENTAL SETUP

A 300 W DC-DC boost converter was built and tests were carried out to investigate the performance of the proposed system. Table 1 lists the boost converter design specifications. Fig. 10 shows the schematic diagram of the test circuit. Power to the test circuit was supplied from two pairs of BP SX3 160S BP solar panels that are each connected in series, and then the pairs are connected in parallel as shown in Fig. 2. The converter components are: a 1.5 mH inductor built from a toroidal core from Magnetics® with a resistance of 500 $m\Omega$, a Panasonic ECA-2WM330 33 μF aluminum electrolytic capacitor with an ESR of 1$m\Omega$, a Vishay IRFP-360 MOSFET used as the power switch (and driven by the output of the TL 494 IN PWM IC) with a switch ON resistance of 200 $m\Omega$, and a DSS17-06CR Schottky diode from IXYS Corporation. The load used was a 1/3 hp series DC motor coupled to a dynamometer. The series DC motor used in the experimental setup had the following parameters: R_m=8Ω, L_m=33mH, J_{motor}=0.0019174 $kg \cdot m^2$, B=0.001 N-ms/rad,

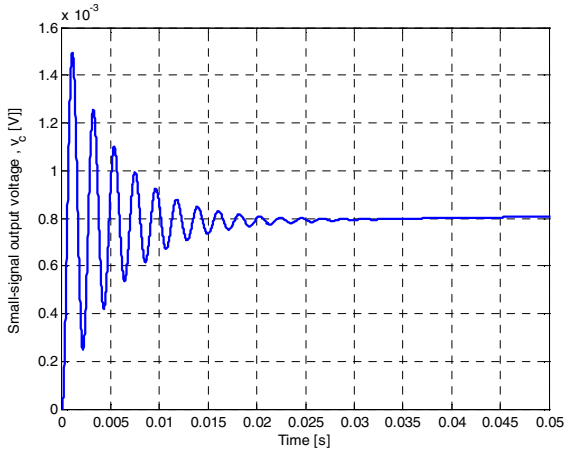

Figure 6. Small-signal component of the output voltage.

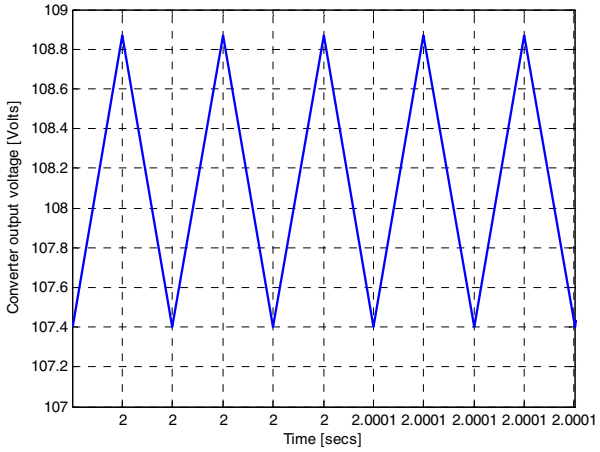

Figure 7. Boost converter output voltage ripple.

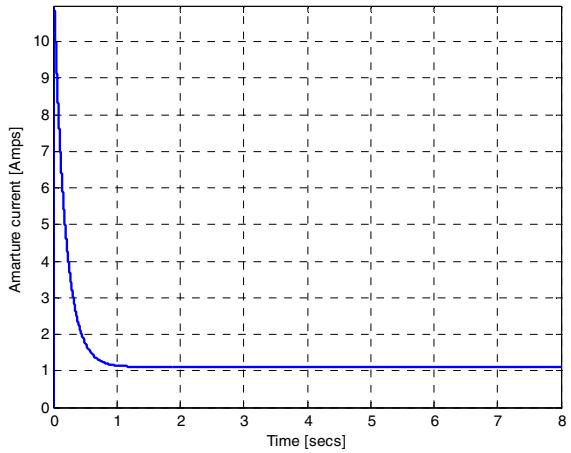

Figure 8. DC motor armature current.

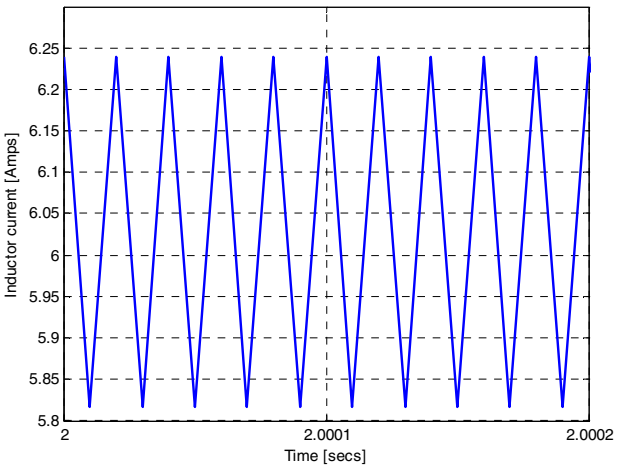

Figure 9. Boost converter inductor current ripple.

K_m=0.67V/rad/s, and ω=1800 RPM nominal. The load was assumed to have the same moment of inertia as the motor. Therefore, the moment of inertia used for simulations was:

TABLE 1. DC-DC BOOST CONVERTER SPECIFICATIONS

Parameter	Value
Output Power	300W
Output Voltage	125V
Input Voltage	60V - 85V
Switching Frequency	50kHz
Output Voltage Ripple	≤ 1%
Inductor Current Ripple	≤ 10%

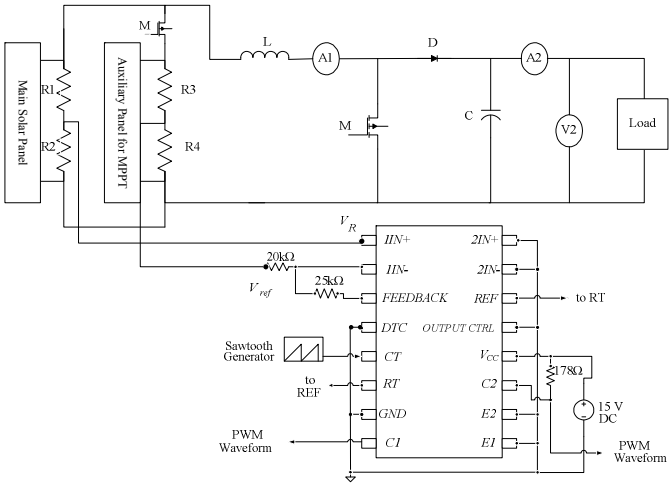

Figure 10. Experimental Test Circuit.

J=J_{motor} +J_{load}=0.003835 $kg \cdot m^2$. Fig. 9 also depicts the ammeters A1 and A2, and the voltmeters V1 and V2 used to measure the input and output characteristics.

The PWM controller comprises the PWM integrated circuit (IC) and the potential divider. The controller chosen for the PWM generation was a TL494 IN from Texas Instruments. The external connections made to this IC for operation are shown in Fig. 10. The error amplifier section of the PWM chip (connected to pins 1IN+ and 1IN-) has an output given by:

$$d = t_{on} f_s . \tag{28}$$

The on-chip oscillator is by-passed by terminating RT to the reference output and providing a sawtooth input to CT. The voltage divider networks provided by R1, R2, and R3, R4 reduce the input and reference voltage to within levels the IC inputs are capable of handling. The resistor values used in the voltage divider networks were as follows: *R1=1MΩ*, *R2=111kΩ*, *R3=1MΩ*, and *R4=111kΩ*. In addition, the R3, R4 network is also used to scale down the open-circuit voltage of the solar panel. The MPP voltage as dictated by the constant voltage MPP algorithm is given by:

$$V_{MPP} = M_V V_{oc} . \tag{29}$$

An M_V value of 0.8 was incorporated into the TL494 IC as was assumed in [15-17].

VII. EXPERIMENTAL RESULTS

The results shown in Fig. 11 and Fig. 12 correspond to the 300W boost converter switched at 50kHz with a series DC motor load. The average value of the solar panel open-circuit voltage used in this experiment was approximately $77V$. The value of the gate signal used to drive the MOSFET was $V_{gs} \approx 14 V_{p-p}$. Fig. 11 shows the DC motor armature voltage

characteristics with the MPP tracker. Also, it can be seen that the output voltage is a little less than the simulation results. This difference can be attributed to extra parasitic elements in the hardware circuit that were not accounted for in the simulation.

Fig. 12 illustrates results obtained from the proposed MPP tracker with a DC motor load. Fig. 12 shows the variation of the input voltage, input power, and boost converter efficiency as a function of the duty cycle. Fig. 12 shows an increasing power extracted from the panel as its output voltage drops towards the end of the curve. This is due to a limitation placed on the inductor design of 5.5 amperes peak current. At about 68 volts, the inductor current averaged 4.8 amperes. Therefore, the system had to be shut down to avoid damage to the entire circuit.

VIII. CONCLUSIONS

In this paper, a constant voltage MPP algorithm was proposed. In the MPP algorithm presented, a switch was connected in series with a pilot array that periodically opens, and the open-circuit voltage was measured. The value of the open-circuit voltage was used as the reference voltage for the PWM modulator. The reference voltage in this scheme was dynamically tracked online, avoiding the need to break the main circuit as done in the conventional constant voltage algorithms. Unlike the conventional algorithm, the proposed version also took into account varying environmental conditions. A 300 W boost converter with a feedforward controller was constructed and interfaced with the solar cell array and the load. The proposed MPP algorithm was verified using a DC motor load. The performance of the interconnected system has been investigated and analyzed. MATLAB/Simulink simulations and experimental analyses were presented to demonstrate the performance of the system. The constant voltage maximum power point (MPP) algorithm presented is a simple (and inexpensive) method to continuously track the MPP of the solar cell array in Fig. 1 as the weather conditions vary.

REFERENCES

[1] E. Trishan, and P. L. Chapman, "Comparison of Photovoltaic Array Maximum Power Point Tracking Techniques," *IEEE Transactions on Energy Conversion* 22, no. 2 (June 2007): 439 – 449.

[2] M.M. Saied, Mohamed Mostafa, "The Available Matching of Solar Arrays to DC Motors Having Both Constant and Series-Excited Field Components," *IEEE Transactions on Energy Conversion* 17, no. 3 (September 2002): 301- 305.

[3] S.M. Alghuwainem, "Performance Analysis of a PV Powered DC Motor Driving a 3-Phase Self-Excited Induction Generator," *IEEE Transactions on Energy Conversion* 11, no. 1 (March 1996): 155-161.

[4] A.K. Abdelsalam, A.M. Massoud, S. Ahmed, and P.N. Enjeti, "High-Performance Adaptive Perturb and Observe MPPT Technique for Photovoltaic-Based Microgrids," *IEEE Transactions on Power Electronics* 26, no. 4 (April 2011): 1010 –1021.

[5] Nicola Femia, Giovanni Petrone, Giovanni Spagnuolo, and Maasimo Viteli, "Optimization of Peturb and Observe Maximum Point Tracking Method," *IEEE Transactions on Power Electronics,* vol. 20, no. 4, (July 2005): 963 – 973.

[6] B.M.T. Ho, H. S. H. Chung, and W. L. Lo, "Use of System Oscillation to Locate the MPP of PV Panels," *IEEE Power Electronics Letters* 2, no. 1 (March 2004): 1-5.

[7] Q. Mei, M. Shan, L. Liu, and J.M. Guerrero, "A Novel Improved Variable Step-Size Incremental-Resistance MPPT Method for PV Systems," *IEEE Transactions on Industrial Electronics,* vol. 58, no. 6 (June 2011): 2427- 2434.

[8] F. Liu, S. Duan, F. Liu, B. Liu, and Y. Kang, "A Variable Step Size INC MPPT Method for PV Systems," *IEEE Transactions on Industrial Electronics* 55, no. 7 (July 2008): 2622-2628.

[9] J.W. Kimball and P. T. Krein, "Digital Ripple Correlation Control for Photovoltaic Applications," *Power Electronics Specialists Conference* (2007): 1690- 1694.

[10] B.M.T. Ho and H. S. Chung, "An Integrated Inverter with Maximum Power Tracking for Grid-Connected PV Systems," *IEEE Transactions on Power Electronics* 20, no. 4 (July 2005): 953-961.

[11] W. Xiao, N. Ozog, and W. G. Dunford, "Topology Study of Photovoltaic Interface for Maximum Power Point Tracking," *IEEE Transactions on Industrial Electronics* 54, no. 3 (June 2007): 1696-1704.

[12] M.A.S. Masoum, H. Dehbonei, and E. F. Fuchs, "Theoretical and Experimental Analyses of Photovoltaic Systems with Voltage- and Current-Based Maximum Power-Point Tracking," *IEEE Transactions on Energy Conversion* 17, no. 4 (December 2002): pp. 514– 522.

[13] A. Tariq and M.S. J. Asgha, "Development of an Analog Maximum Power Point Tracer for Photovoltaic Panel," *IEEE Power Electronics and Drives Systems* (2005): 251-255.

[14] K.M. Kazimierczuk and L. A. Starman, "Dynamic Performance of PWM DC-DC Boost Converter with Input Voltage Feedforward Control," *IEEE Transactions on Circuits and Systems—I: Fundamental Theory and Applications* 45, no. 12 (December 1999): 1473-1481.

[15] Nicola Femia, Gianpaolo Lisi, Giovanni Petrone, Giovanni Spagnuolo, and Maasimo Viteli, " Distributed Maximum Power Point Tracking of Photovoltaic Arrays: Novel Approach and System Analysis," *IEEE Transactions on Industrial Electronics,* vol. 55, no. 7 (July 2008): 2610 – 2621.

[16] K.K. Tse, B. M. T. Ho, H. S. Chung, and S. Y. R. Hui, "A Comparative Study of Maximum-Power-Point Trackers for Photovoltaic Panels Using Switching-Frequency Modulation Scheme," *IEEE Transactions on Industrial Electronics* 51, no. 2 (April 2004): 410-418.

[17] N. Mohan, T. M. Undeland, and W. P. Robbins, *Power Electronics: Converters Applications, and Design.* John Wiley & Sons, Inc., 2003.

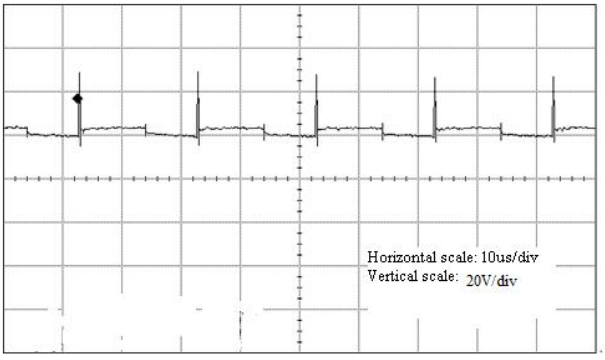

Figure 11. DC motor armature voltage.

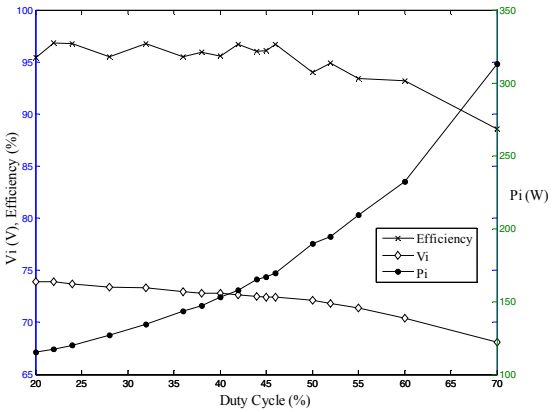

Figure 12. Measured solar panel characteristics versus switch duty cycle.